water

MDPI

Article

Study on Adsorption of As(III) by a New Bio-Material from Chitin Pyrolysis

Zhiguang Yang [1], Gaojun Yan [1,2,3], Zhiwei Song [2], Junzheng Zhang [1], Chenlong Wang [1], Zhisheng Yu [3], Zhihui Bai [3], Guoqiang Zhuang [3] and Feng Liang [1,*]

1 Henan Province Key Laboratory of Water Pollution Control and Rehabilitation Technology, Henan University of Urban Construction, Pingdingshan 467036, China; yangzhiguang@hncj.edu.cn (Z.Y.); gjyan1995@163.com (G.Y.); 18768913062@163.com (J.Z.); wulisy@outlook.com (C.W.)
2 School of Environmental and Chemical Engineering, Heilongjiang University of Science and Technology, Harbin 150022, China; szwcyp@163.com
3 Laboratory of Environmental Biotechnology, Research Center for Eco-Environmental Sciences, Chinese Academy of Sciences, Beijing 100085, China; yuzs@ucas.ac.cn (Z.Y.); zhbai@rcees.ac.cn (Z.B.); gqzhuang@rcees.ac.cn (G.Z.)
* Correspondence: liangfeng@hncj.edu.cn; Tel.: +86-106-284-9155

Abstract: Chitin-char is obtained from fast pyrolysis of chitin. To obtain the maximum surface area, chitin-char is treated by nitric acid. Then, a kind of new arsenic removal bio-material is prepared by loading $Ca(OH)_2$ on the char (called $Ca(OH)_2$-char). IR spectroscopy before and after char treatment reveal at least three distinct patterns of peak changes. An adsorption study is performed at different doses, pHs, and coexisting ions in the batch mode. The adsorption kinetics follows two first-order equations. Kinetic studies yield an optimum equilibrium time of 2 h with an adsorbent dose of 0.4 g/L and concentration of 10 mg/L. Using only 0.4 g/L of carbon, the maximum removal capacity is about 99.8%. The result indicates that the $Ca(OH)_2$-char has a high adsorption capacity in the process of removing arsenic (III).

Keywords: bio-materials; arsenic; adsorption; water treatment

check for updates

Citation: Yang, Z.; Yan, G.; Song, Z.; Zhang, J.; Wang, C.; Yu, Z.; Bai, Z.; Zhuang, G.; Liang, F. Study on Adsorption of As(III) by a New Bio-Material from Chitin Pyrolysis. *Water* **2021**, *13*, 2944. https://doi.org/10.3390/w13212944

Academic Editors: Laura Bulgariu, Wei Zhao, Xiaoyan Liu, Yukun Zhu and Feihu Mu

Received: 14 September 2021
Accepted: 14 October 2021
Published: 20 October 2021

Publisher's Note: MDPI stays neutral with regard to jurisdictional claims in published maps and institutional affiliations.

Copyright: © 2021 by the authors. Licensee MDPI, Basel, Switzerland. This article is an open access article distributed under the terms and conditions of the Creative Commons Attribution (CC BY) license (https://creativecommons.org/licenses/by/4.0/).

1. Introduction

Arsenic has harmful effects on humans, plants and animals. Incidents of arsenic contamination in groundwater have been reported all over the world [1]. Chronic exposure to arsenic concentrations above 100 µg/L can cause vascular disorders, such as dermal pigments (Blackfoot disease) and skin, liver and lung cancer [2,3].

In water, it is commonly found in inorganic arsenic species, such as arsenite (AsO_3^{3-}) and arsenate (AsO_4^{3-}), referred to as As(III) and As(V), respectively. Greater attention is required for the removal of As(III) from groundwater due to its higher toxicity and mobility, which mainly arise from its neutral state (H_3AsO_3) in groundwater as compared to the charged As(V) species ($H_2AsO_4^-$, $HAsO_4^{2-}$), which predominate near pH 6–9 [4–7]. This also correlates with the less efficient removal of As(III) by conventional water treatment processes [8].

Application of adsorbents for removal of arsenic has drawn attention due to higher adsorption capacity and repetitive use of the material. Among those adsorbents, iron oxide-based adsorbents, for example, granular ferric hydroxide, are highly efficient for As(III) removal [9]. The agricultural by-products and/or bio-materials are also of the utmost importance because of their low cost, availability and reasonably high adsorption capacities. A wide range of agricultural by-products and bio-materials have so far been studied in the view of determining efficient and cost-effective adsorbents. Red mud [10], blast furnace slag [11], bio-char [12–17], iron oxide [18,19], nano-iron and iron-loaded activated carbon [20,21] and so forth have been studied by the researchers, considering

their prospect to be converted as adsorbents. Chitin [22–24], the second-most abundant natural polysaccharide, is widely spread in shells of crabs, shrimps, insects, fungal cell wall, etc. It is mainly composed of the acetylglucosamine units (the acetamido group at the C-2 position). Being a renewable and biodegradable material that currently has few uses, chitin plays a significant role in state-of-the art-research in an attempt to valorize it and replace non-renewable materials. The chitin-char properties differ from those of lignocellulose-char due to its acetamido group, which are influenced by various factors, such as surface area, functional groups, cation and anion content, etc. These properties usually lead to high adsorption, and hence, the char as an adsorbent material becomes possible.

Kinetics is an important subject in the research of adsorption. Different kinetic models based on analysis of adsorption processes were established [25–27]. However, the effects of such parameters as adsorbate, adsorbent, temperature, pH, etc. on adsorption processes are so complicated that there is no universal adsorption rate equation [28–32].

In the present study, chitin was fast pyrolyzed in a tubular furnace pyrolysis reactor (500 g/batch) under such conditions as 390 °C and 6×10^{-2} Pa. The basic objectives of the present investigation have been:

(1) Obtaining a maximum surface area; showing the influence of common ions (NaCl, $NaHCO_3$ and Na_2SO_4).
(2) Demonstrating arsenic removal by char from water/wastewater at different pHs.
(3) Obtaining adsorption kinetics to establish the mechanism.

2. Materials and Methods

2.1. Pyrolysis of Chitin

Chitin-chars were produced by pyrolyzing chitin (buy from Golden-Shell Pharmaceutical Co., Ltd, Yuhuan, China) in a tubular furnace pyrolysis reactor. The pyrolysis apparatus used has been previously described [33,34]. It was dried at 60 °C before pyrolysis for 2 h. Each feed was ground and sieved to a particle size of 2–6 mm before use. The pyrolysis temperature of 390 °C and vacuum pressure of 6×10^{-2} Pa was adopted during the process of pyrolysis. The char was ground and sieved to a particle size of 1–3 mm before use.

2.2. Treatment with Nitric Acid

The char from chitin pyrolysis was further treated by HNO_3 with a concentration of 1–20 wt. %. The mixture with a solid to liquid ratio of 1:5 was refluxed for 1 h, and then solid was collected by filtration, washed with water until the filtrate tested neutral to pH paper and dried to constant weight at about 105 °C. Char was sieved, and the particle size fraction from 20 to 32 meshes was subsequently characterized and further used.

2.3. The preparation of $Ca(OH)_2$-Loaded Chars

Ten grams of HNO_3-treated chars in a sealed glass bottle were soaked in 100 mL of $Ca(OH)_2$ solutions with a series of concentrations (0.025, 0.05, 0.075, 0.1 and 0.15 wt. %) for 1 h at 100 °C and then unsealed, evaporated and dried to constant weight at about 105 °C. Thus, chars with a series of base capacities (i.e., the content of $Ca(OH)_2$ in char is 2.5, 5, 7.5, 10, 15 mg/g) were developed by the addition of $Ca(OH)_2$.

The chars before and after loading were analyzed by infrared spectroscopy on a Thermo Electron Corporation IR 300 spectrometer (Thermo Electron Corporation, Waltham, MA, USA) between 400 and 4000 cm^{-1}, with 50 scans being taken at 2 cm^{-1} resolution. Char samples were ground in an agate mortar and then mixed with KBr (Merck KGaA, Darmstadt, Germany, for spectroscopy) at an approximate ratio of 1/400. Pressing at 10 t/cm^2 for 3 min with a Perkin–Elmer hydraulic press (PerkinElmer Instruments Co. Shanghai, China), under vacuum generated pallets. The spectrum of a similar thickness KBr pellet was used as background.

2.4. Reagents and Equipment

Reagents were all AR-grade. Stock solutions (1000 mg/L) of the test reagents were made by dissolving $NaAsO_2$, in deionized water. Feeding solutions were prepared by the dilution of stock solutions, and their pH was adjusted to 8.0 with nitric acid (0.1 N) or sodium hydroxide (0.1 N).

The pH measurements were made using an Orion pH meter (Thermo Electron Corporation, Waltham, MA, USA).

The concentration of arsenic in solution was determined on an atomic fluorescence spectrophotometer (PF6, Puxitongyong Instrument Corp., Beijing, China) coupled with a hydride generator. The detection limit of the instrument is 0.1 µg/L. Sample blanks were analyzed for correction of background effect on instrument response.

Chars were characterized by a surface area and pore size analyzer (Micromeritics ASAP 2020 Surface Area and Porosity Analyzer Software V3.00, Micromeritics instrument Ltd). The N_2 isotherms were determined in. About 0.10 g of sample was outgassed at 250 °C for 12 h, prior to effecting adsorption measurements.

2.5. Adsorption Procedure

Batch adsorption studies were performed to obtain both rate and equilibrium data. Bottles (250 mL) were filled with 100-mL solutions of As(III) (10 mg/L) for kinetic investigation. Other dilute solutions containing arsenic (10 mg/L) were dispensed in 20-mL aliquots in 50-mL Erlenmeyer flasks (Sichuan Shubo co. Ltd, Chengdu, China), and then they were shaken in a rotary shaker at 200 rpm at 25 °C, and the necessary analyses were made during the adsorption period. Adsorption studies were performed at different adsorption doses, pHs, coexisting ions, and adsorption time. A known amount of $Ca(OH)_2$-char was added to each bottle followed by shake for specified times to a maximum of 12 h. The contact time and conditions were selected based on preliminary experiments, which demonstrated that equilibrium was established in about 2 h for 10 mg/L. After this period, solutions were filtered using a 0.2 membrane filter (Millipore Corporation, Burlington, MA, USA), and the remaining concentrations of arsenic were determined. The adsorbed arsenic was calculated by difference between the initial and equilibrium concentrations in solution.

2.6. Effect of Coexisting Ions

The effect of common ions (NaCl, $NaHCO_3$ and Na_2SO_4) on the adsorption of arsenic onto the $Ca(OH)_2$-char was investigated. The molar ratio of them to arsenic was 1–10:1. Twenty milliliters of arsenic solution (10 mg/L) with added ions was adjusted to pH 8.5 and mixed with 40 mg $Ca(OH)_2$-char with $Ca(OH)_2$ capacity of 15 mg/g. The mixtures were equilibrated at 25 °C for 6 h with mild shake (200 rpm) and the concentration of residual arsenic was analyzed.

2.7. Kinetic Studies

At 25 °C, 2 g of $Ca(OH)_2$-char was added to stoppered flasks (250 mL) containing 100-mL solutions of arsenic (10 mg/L) in a mild shaker (200 rpm). Samples were taken at different time intervals and analyzed.

2.8. Quality Control

All batch isotherm tests were replicated three times, and the blanks were run in parallel to establish accuracy, reliability and reproducibility. All glassware was presoaked in a 10% HNO_3 solution, rinsed with deionized water and oven-dried. Blanks were run and corrections applied if necessary. All solutions analyzed were filtered using membrane filters with a 0.45-µm pore size. All the observations were recorded in triplicate, and average values are reported.

3. Results and Discussion

3.1. Specific Surface Area

As represented in Figure 1, the surface area has a lower value (32.9 m^2/g) for the initial chitin-char; after 1% HNO_3 treatment 1 h, the value sharply increases to 283 m^2/g. The difference could be due to the removal of considerable pyrolysis by-products (especially minerals) present in the char surface, which could cause pore blockage. The surface area reaches the highest value (342 m^2/g); after that, the value gradually decreases with the increase in nitric acid concentration. The phenomenon can be explained in such a way that the pore structure is partly destroyed, which results from excessive oxidation of surface carbon because of higher nitric acid concentration. Based on this, 10% HNO_3-treated char was subsequently used as the $Ca(OH)_2$-loaded material.

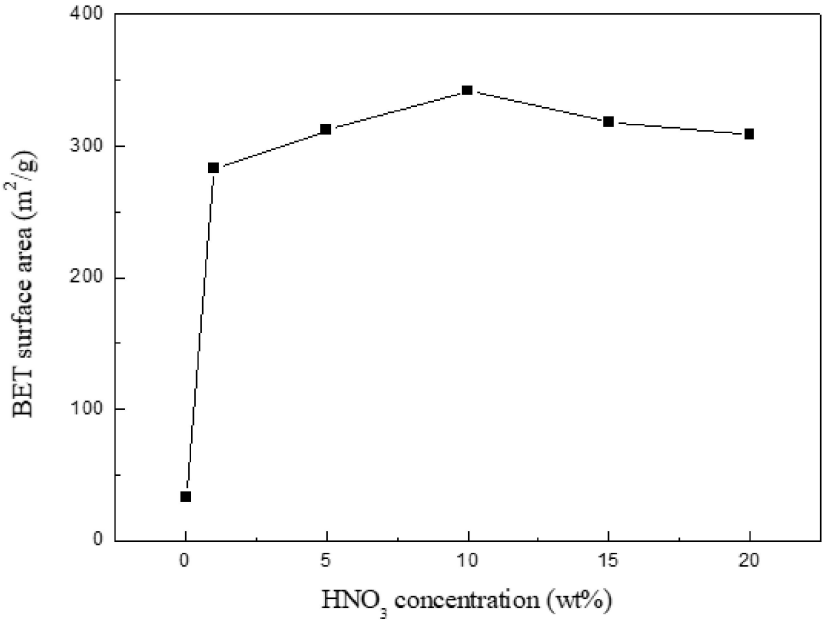


Figure 1. BET surface area of chitin-char treated by HNO_3 of different concentration.

3.2. Adsorption Experiments for Different Samples

The rate of As(III) uptake was studied versus the HNO_3-treated chars without $Ca(OH)_2$ or with 2.5, 5, 7.5, 10, or 15 mg/g of $Ca(OH)_2$ (Figure 2). From Figure 2, the uptake rate increases as the amount of $Ca(OH)_2$ increases. The adsorption rate reaches the highest value (99.8%) for the char with 10 mg/g of $Ca(OH)_2$. Arsenic removal of the HNO_3-treated chars without $Ca(OH)_2$ has only 56.2%. A further experiment states the original char before the HNO_3 treatment has worse adsorption (merely about 28%) than those treated chars. So, 10% HNO3-treated char with 10 mg/g of $Ca(OH)_2$ was subsequently used as the adsorption material.

3.3. IR Characterization

The infrared spectra of the carbonaceous adsorbents are shown in Figure 3. These display bands due to different oxygen-containing surface groups (C=O, C–O, –OH) and others (C-NH, $–CH_2$, NH_2, aromatic rings). These possible peaks are listed in Table 1. Their spectra are similar in shape and in their intensities. Since chitin was charred at relatively low temperatures, only partial aromatization occurred. A band at 3692 cm^{-1} appears at the high wavenumber that can be allocated to free hydroxyl groups. A new band (1716 cm^{-1}) is observed in the spectrum of HNO_3-treated char that denotes a certain amount of carboxylic acids, which should partly be from nitric acid oxidation. The band (1716 cm^{-1}) disappears in the spectrum of $Ca(OH)_2$-loaded char that shows carboxylic acid is an active group of adsorption. In spectrum 3, there is also a small band just above

1500 cm^{-1} that might be from the newly formed carboxylate anion, whereas bands that are related to amide and which are more present in initial char and the $Ca(OH)_2$-loaded one are reduced or disappear: 1430 and 870 cm^{-1} by ammonium nitrate. The bands near 1022 cm^{-1} were due to the stretching vibration of C–O bond from C=O because of cations addition.

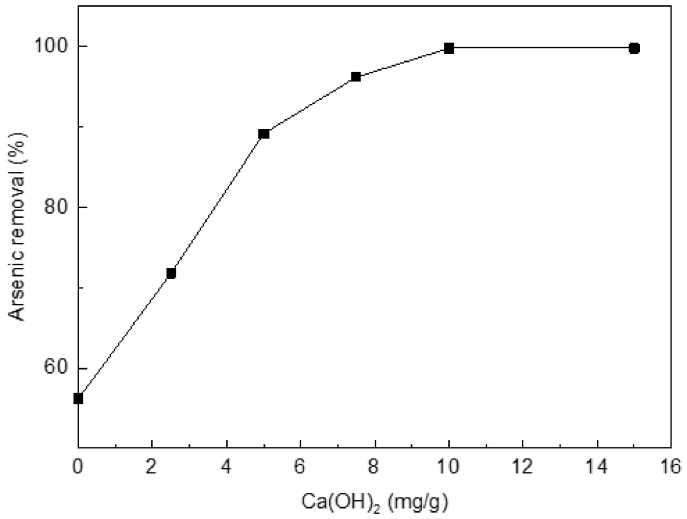


Figure 2. Effect of loading $Ca(OH)_2$ on arsenic(III) adsorption. Initial [As]: 10 mg/L; pH: 8.5; temperature: 25 °C; equilibration time: 12 h.

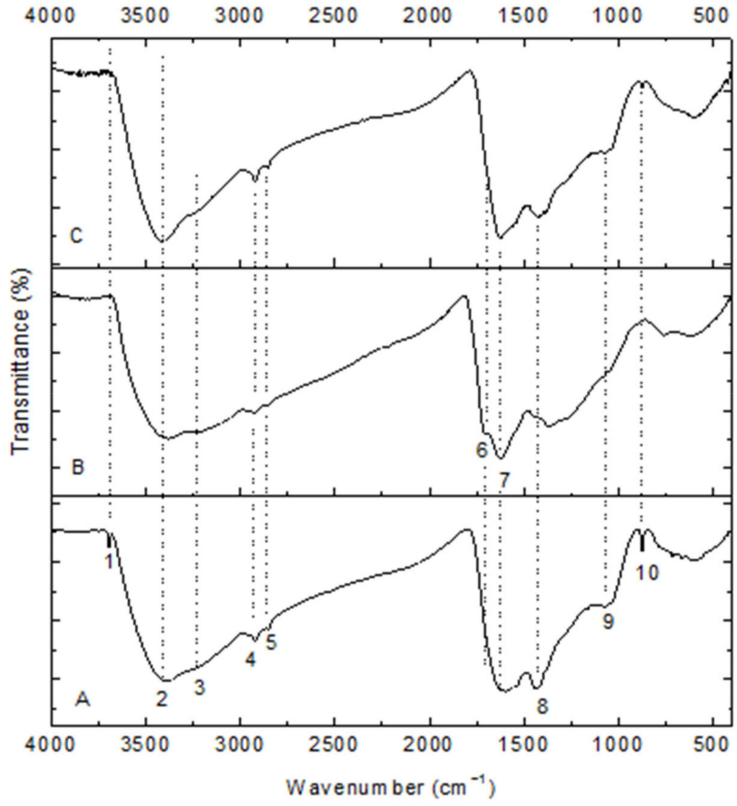


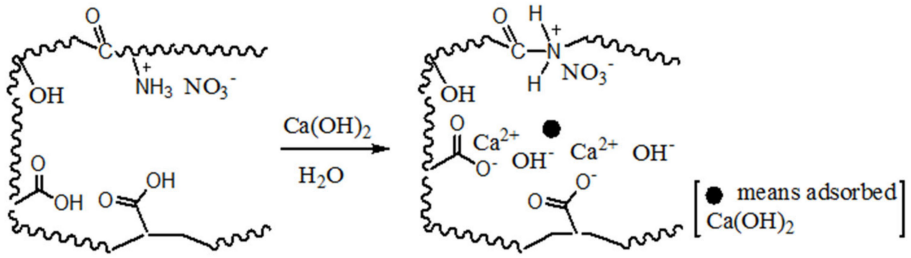
Figure 3. FT-IR spectra of chars. (**A**) chitin-char; (**B**) HNO_3-treated char; (**C**) $Ca(OH)_2$-char.

Table 1. Analysis for FT-IR spectra of chars.

Number	Wave (cm^{-1})	Explanation of Band	Sample
1	3692	O-H	A
2	3420	Hydroxyl stretching	A, B, C
3	3250	N–H stretching in amine	A, B, C
4	2920	C–H stretching	A, B, C
5	2850	C–H stretching	A, B, C
6	1716	C=O stretching (carboxylic acid)	B
7	1625	N-H bending in amine	A, B, C
8	1430	C–N stretching and/or C–H deformationsand/or C=C stretching in aromatic rings	A, C
9	1022	C–O stretching	A, C
10	870	C-N bending	A, C

These groups (hydroxyl, carboxylic acid, amine) on the char confer significant hydrophilic character, which aids the fast diffusion and removal of ionic solutes from aqueous solution because of little internal transfer resistance.

To clearly elucidate the surface groups and mechanism of $Ca(OH)_2$ load, Scheme 1 shows these hydrophilic groups and the process of $Ca(OH)_2$ load. According to the adsorption state, two adsorption models are established, ion-absorbing type and precipitation type. This highlights that the pore structure of the adsorbent is effectively helpful to home position ion exchange or crystallization.



Scheme 1. Inferred mechanism of precipitation and ion-absorbing for $Ca(OH)_2$ load on chars.

3.4. Adsorption Studies

The rate of As(III) uptake was studied versus char dose at 0.02, 0.05, 0.1, 0.2, 0.4, 0.8 and 1.0 g/L (Figure 4). The uptake rate increases as the amount of char increases. The adsorption rate increases substantially when the dosage increased from 0.02 to 0.4 g/L. Therefore, char dose was held at 0.4 g/L in all studies. For 0.4 g/L char dose, the adsorption capacity is 24.95 mg/g more than the values reported in the literature, such as Biochar produced from municipal solid wastes (24.49 mg/g) [35], cattle bone char (0.399 mg/g) [36], perilla leaf biochar (7.21 mg/g) [37], peanut shell biochar (7.94 mg/g) [38] and Virgin coniferous wood biochar (1.8 mg/g) [14]. Arsenite content of solution decreased from 10 mg/L to 0.02 mg/L close to the World Health Organization's Guidelines for Drinking-water Quality (0.01 mg/L).

Experiments were conducted to determine the optimum pH for the arsenic uptake by $Ca(OH)_2$-chars (Figure 5). Initial concentration of 10 mg/L was used. The greatest adsorption occurred at pH 8–11. Thus, all experiments were subsequently conducted at pH 8.5.

Neutralization and precipitation are two competitive parallel processes at lower pH values. Neutralization of H^+ and OH^- is predominant at lower pH values that lead to lower arsenic removal. Additionally, smaller adsorption values observed at low pH are also attributed to diffusion competition between the nitrate and arsenic ions, OH^- released by chars into the solution. At high pH values, arsenic removal from solution is enhanced by metal oxide precipitation. The lowest concentration of arsenic (III) is about 0.3 mg/L

and is reached when the solution is saturated with $Ca(OH)_2$ [39]. The value may be lower because of profitable metal oxide precipitation due to adsorption.

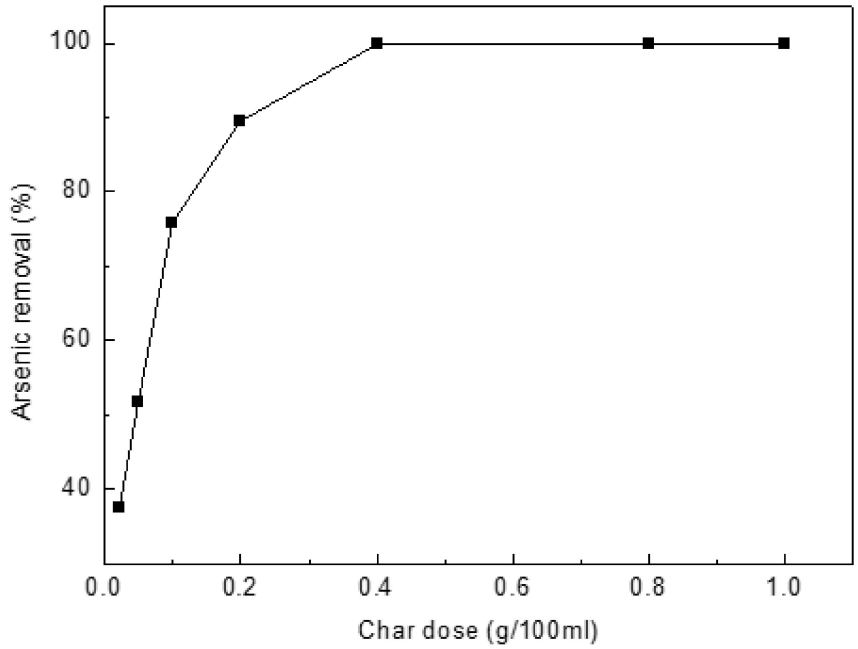


Figure 4. Effect of char dose on arsenic(III) adsorption. Initial [As]: 10 mg/L; pH: 8.5; temperature: 25 °C; equilibration time: 12 h.

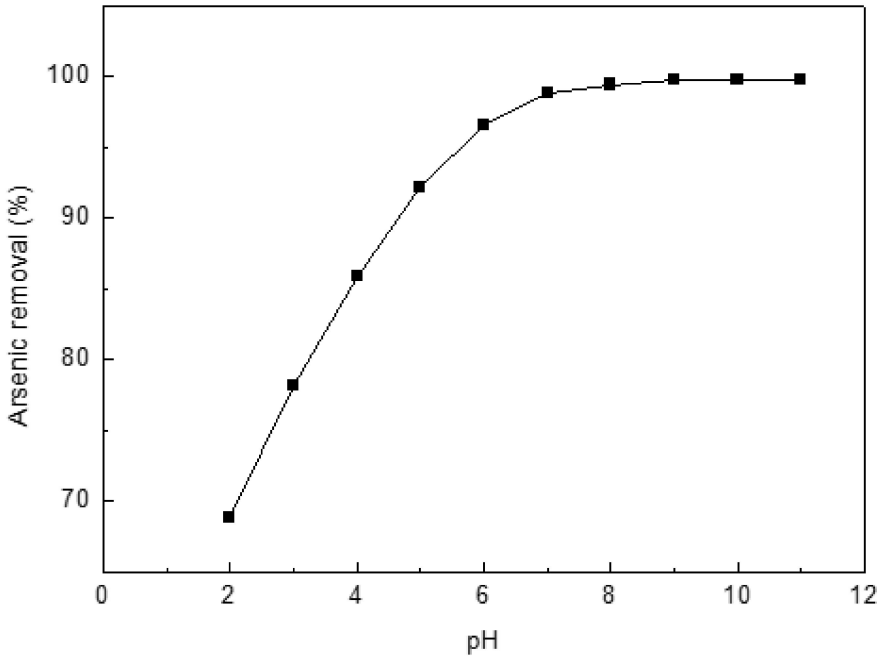


Figure 5. Effect of pH on the adsorption of arsenic on char. Initial arsenic concentration: 10 mg/L; char: 0.4 g/L; temperature: 25 °C; equilibration time: 12 h.

The dominant species of arsenic in aqueous solution correlates closely with pH of the solution. Trivalent arsenic is stable at pH 0–9 as neutral H_3AsO_3, while $H_2AsO_3^-$, $HAsO_3^{2-}$ and AsO_3^{3-} exist as stable species in the pH intervals 9–12, 12–13 and 13–14, respectively [39,40]. While $Ca(OH)_2$–char was added to arsenic solution, all pores of char were instantly filled with water, and saturated $Ca(OH)_2$ solution was first produced in

pores, which should have higher pH values (should be above 12) than feed solution; thus, precipitation should be $CaAsO_2OH{\cdot}1/2H_2O$ based on references [39,41].

Figure 6 shows the effect of common ions Cl^-, HCO_3^- and SO_4^{2-} (NaCl, $NaHCO_3$ and Na_2SO_4) on the adsorption of arsenic onto the $Ca(OH)_2$-char. The Cl- ion at molar ratios up to 10 has no effect on As(III) uptake, whereas arsenic adsorption decreases with increasing molar ratio of ions to arsenic from 99.8 to 46.9% and 82.8% for HCO_3^- and SO_4^{2-}, respectively. Such behavior of As(III) adsorption in presence of interfering ions should be due in large part to producing $CaCO_3$ or $CaSO_4$ not dissolved in water. It is informative for in-situ remediation using $Ca(OH)_2$-char due to the coexistence of competing anions in natural groundwater. That is, more doses should be necessary in practical application.

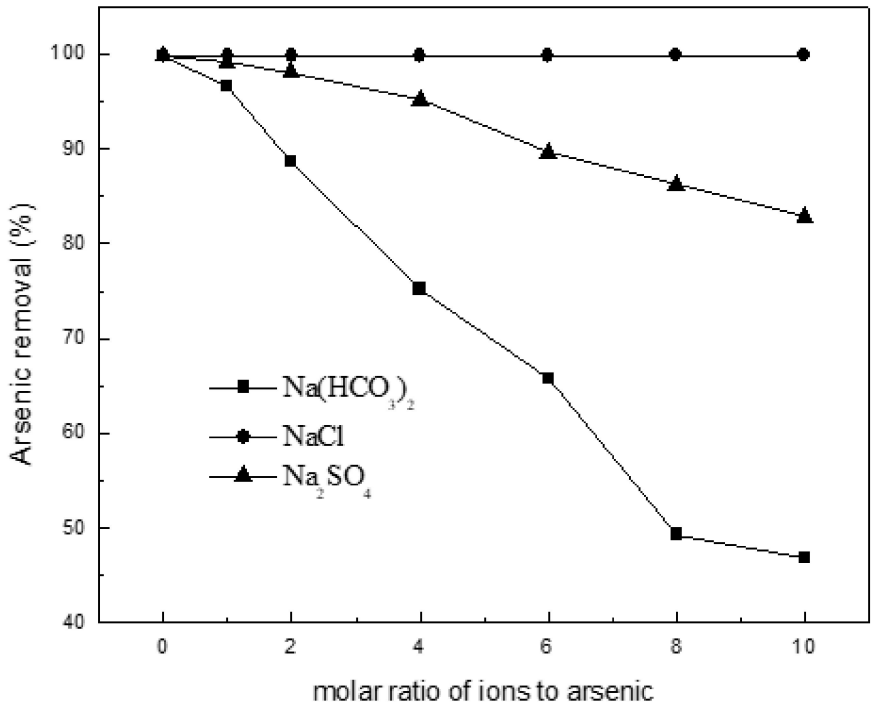


Figure 6. Effect of coexisting ions on the adsorption of arsenic on char. Initial arsenic concentration: 10 mg/L; char: 0.2 g/L pH: 8.5; temperature: 25 °C; equilibration time: 12 h.

3.5. Adsorption Mechanism

Three-stage adsorption mechanism had been described by other researchers [42,43]. In the 3-stage model, such different stages as the external surface adsorption, the gradual adsorption and the final equilibrium stage were considered based on the fit of time $t_{1/2}$. In fact, different adsorptions should take place simultaneously during the whole process.

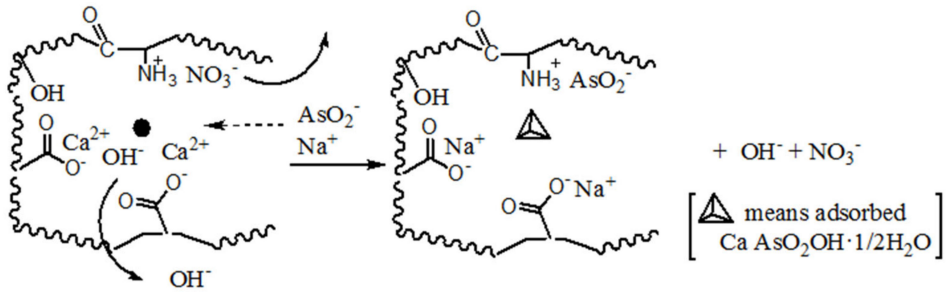
To further understand the adsorption mechanism of arsenic, the final pH value at adsorption equilibrium has been measured, and its value is 11.1. The rise of pH in the system must be due to the exchange interaction between char and solution. This indicates that the adsorption is dominated by an ion-exchange mechanism during the entire adsorption period. Substantial hydroxyl ions in the pore of char are released into the solution by ion exchange; by contrast, AsO_2^- diffuses from feed solution into the pore, and then Ca^{2+} or amine is able to take part in the reactions in the following manner:

$$nCa(OH)_2 + nAsO_2^- + n/2H_2O = n\,CaAsO_2OH{\cdot}1/2H_2O + nHO^- \quad (1)$$

$$nC\text{-}CNH_3(NO_3) + nAsO_2^- = nC\text{-}CNH_3(AsO_2) + nNO_3^- \quad (2)$$

These reactions lead to solution basification during adsorption. Excessive accumulation of AsO_2^- is capable of reacting with calcium ion to form precipitates, and they are adsorbed in pores as a reaction formula (1). Thus, home position crystallization is

considered to be the predominant adsorption mechanism on the $Ca(OH)_2$-chars during the adsorption period. Additionally, amine can adsorb AsO_2^- from solution through ionic exchanging as reaction Formula (2). These reactions are fast due to high calcium ion concentration and plentiful amine in pores so that reaction rates are higher than the diffusion in the initial stage. The reaction rate decreases with the decrease in calcium ion concentration in pores until the reaction rate and the diffusion of AsO_2^- are equal. The adsorption rate reaches the highest level at this time. Here, the rate is called the extreme adsorption rate, which is represented symbolically by rec, the time is called the characteristic adsorption time, which is represented symbolically by tec and the AsO_2^- concentration is called characteristic adsorption concentration, which is represented symbolically by Cie. After that, the reaction rate and the diffusion of AsO_2^- will always be equal, and the reaction rate decreases with decreasing concentrations of AsO_2^- to new adsorption equilibrium. Thus, there are two stages (initial and final stages) during the entire adsorption process. The ion exchange behavior is presented in Scheme 2.



Scheme 2. Inferred mechanism of home position crystallization and ion exchange for arsenic adsorption onto $Ca(OH)_2$-loaded chars.

3.6. Kinetic Studies

The kinetic treatment is based on six assumptions as shown below:

(4) There is a maximum adsorption rate during the entire adsorption process, and the adsorption rate gradually increases with increasing porous AsO_2^- concentration in the initial stage; after that, the adsorption rate gradually decreases with decreasing AsO_2^- concentration in the final stage.

(5) While $Ca(OH)_2$–char was added to arsenic solution, all pores of char were instantly filled with water, namely initial diffusion of water molecule is negligible because of its good hydrophilicity. After that AsO_2^- rapidly diffuses into pores from solution and reaches an equilibrium concentration between outside and inside pores.

(6) In the initial stage, concentration of Ca^{2+} in pore is higher and close to $Ca(OH)_2$ saturated water solution.

(7) Home position crystallization is the predominant adsorption mechanism on the chars during initial adsorption period and adsorption rate depends on the concentration of AsO_2^- in pore from initial zero to an equilibrium concentration (C_{ie}). After that, the concentration of AsO_2^- in pores decreases because of further ion-exchange reaction.

(8) Ion-exchange is the predominant adsorption mechanism during the final adsorption period and adsorption rate depends on the concentration of AsO_2^- in pores from the initial equilibrium concentration C_{ie} to the final equilibrium concentration (C_{fe}).

(9) The rate of deadsorption is negligible compared to the rate of adsorption.

Figure 7 shows arsenic removal measured as a function of time. The arsenic concentrations range from 10 to about 0 mg/L in solution during the adsorption process. The equilibrium concentration is 4.952 mg/L, while the maximum adsorption rate is 0.2064 mg/L/min at 50 min. Based on the above assumptions, there is an equilibrium between inside and outside pores in the initial stage, and the arsenic concentrations in

pores range from 0 to about 5 mg/L. The adsorption rate of arsenic is directly related to the change of arsenic concentrations in pores. That is,

$$\frac{dC}{dt} = k_1 C_t \tag{3}$$

where C_t is arsenic concentration in pores at time t ($t = t_0$ to t_{ie}, $t = t_0$ while $C_0 = 0$ mg/L; $t = t_{ie}$ while $C_{ie} = 4.95$ mg/L), and k_1 is a rate constant in the initial stage. Integration of (3) gives,

$$ln(C_{ie}/C_t) = k_1(t_{ie} - t) \tag{4}$$

where t_0 is the initial time, C_0 is the initial concentration in pores, t_{ie} is the initial equilibrium time and C_{ie} is the initial equilibrium concentration. The value calculated for k_1 is 0.0416 min^{-1} (0.206 ÷ 4.95) for the concentration range used in this investigation.

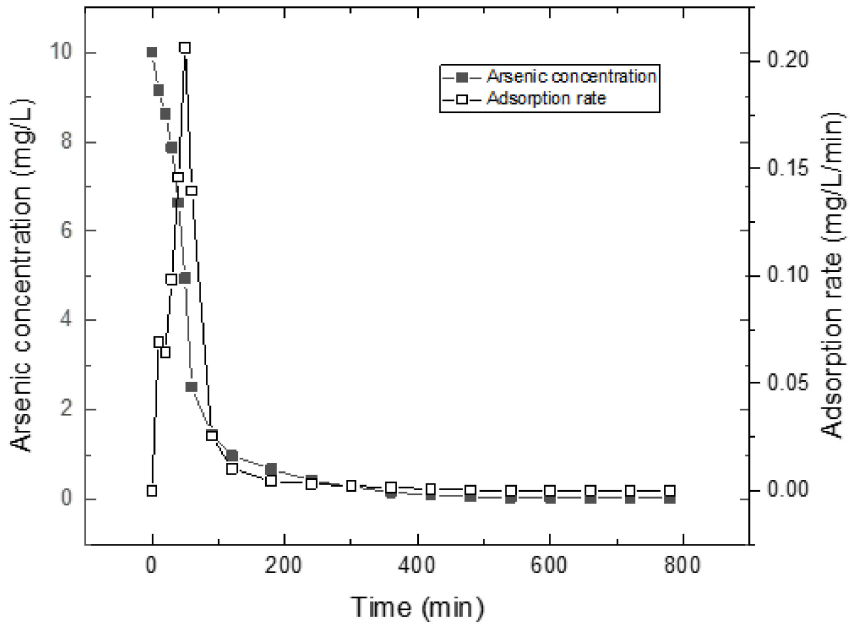


Figure 7. Arsenic removal measured a as a function of time.

Thus,

$$C_t = C_{ie} e^{0.0416(t - t_{ie})} \tag{5}$$

In the final stage, the adsorption rate of arsenic is directly related to the change of arsenic concentrations in solution. That is,

$$-\frac{dC}{dt} = k_2\left(C_t - C_{fe}\right) \tag{6}$$

where C_t is arsenic concentration in solutions at time t ($t = t_{ie}$ to t_{fe}, $t = t_{ie}$ while $C_{ie} = 4.952$ mg/L; $t = t_{fe}$ while $C_{fe} = 0.036$ mg/L), and k_2 is a rate constant in the final stage. Integration of (6) gives,

$$ln[\left(C_t - C_{fe}\right)/\left(C_{ie} - C_{fe}\right)] = -k_2(t - t_{ie}) \tag{7}$$

The value calculated for k_2 (Table S1 in Supplementary Materials) is 0.011 min^{-1} for the concentration range used in this investigation.

Thus,

$$C_t = C_{fe} + \left(C_{ie} - C_{fe}\right) e^{-0.011(t - t_{ie})} \tag{8}$$

The change of arsenic concentration is directly proportional to arsenic removal. Thus, after normalization (5),

$$R_t = R_{ie} e^{0.0416(t-t_{ie})} \quad (9)$$

where R is percentage of arsenic removal at time t and R_{ie} is percentage of arsenic removal at the initial equilibrium ($t = t_0$ to t_{ie}, $t = t_0$ while $R_0 = 0$; $t = t_{ie}$ while $R_{ie} = 74.85\%$). (8) gives,

$$R_t = R_{fe} + \left(R_{ie} - R_{fe}\right) e^{-0.011(t-t_{ie})} \quad (10)$$

where R_{fe} is percentage of arsenic removal at the final equilibrium. ($t = t_{ie}$ to t_{fe}, $t = t_{ie}$ while $R_{ie} = 74.85\%$; $t = t_{fe}$ while $R_{fe} = 99.64\%$).

Plotting $ln(R_t)$ versus "t" provided the second-order adsorption rate constant (k_1 or k_2) and equilibrium values (R_{ie} or R_{fe}) from slopes and intercepts (figure omitted for brevity). Their correlation coefficients for the linear plots are superior (>0.99). Clearly, theoretical and experimental values have an excellent agreement (Figure 6). Thus, arsenic concentration inside and outside the pore model can be considered, and the adsorption process is two first-order diffusions. The model assumes that the adsorption rate depends on the concentration of adsorbate in pores, whereas the surface of adsorbent is not considered. Thus, the model is obviously different from the traditional adsorption models. It makes a new attempt on the kinetic model of adsorption.

Kinetic investigations of As(III) uptake on $Ca(OH)_2$–chars confirmed that adsorption is quite rapid. Typically, about 70% of the ultimate adsorption occurs within the first hour. This is followed by a very slow approach to equilibrium. Saturation is almost reached in 12 h (Figure 8).

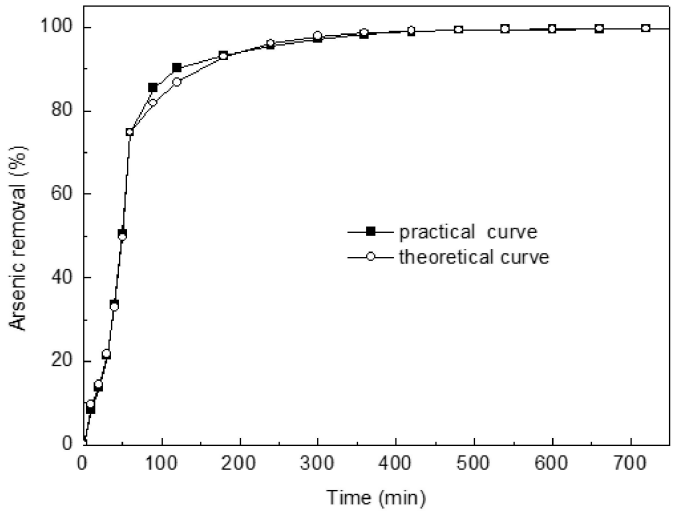


Figure 8. Comparison between experimental and theoretical kinetic curves.

4. Conclusions

Chitin-char was prepared as new arsenic (III) removal bio-material with the absorption capacity about 20 mg/g. The adsorption process can be divided into two stages, and it is controlled by diffusion of arsenic from solution into pore. The adsorption rate increases from zero to the highest level in the initial stages, by contrast, from the highest to zero in the second stage. The new kinetic equation was presented to describe the whole adsorption process by introducing the characteristic adsorption concentration C_{ie}. The characteristic concentration should be closely related to the adsorption parameters (especially the temperature, the nature of adsorbate and adsorbent, etc.).

Supplementary Materials: The following are available online at https://www.mdpi.com/article/10.3390/w13212944/s1, Table S1: Calculation of k_2.

Author Contributions: Conceptualization, Z.Y. (Zhiguang Yang), Z.S. and F.L.; methodology, Z.Y. (Zhisheng Yu) and F.L.; experimental design, Z.Y. (Zhiguang Yang), G.Y. and F.L.; formal analysis, Z.Y. (Zhisheng Yu) and F.L.; investigation, Z.Y. (Zhiguang Yang), G.Y., J.Z. and C.W.; resources, Z.S. and G.Z.; writing-original draft preparation, Z.Y. (Zhiguang Yang) and G.Y.; writing-review and editing, Z.Y. (Zhiguang Yang), G.Y., J.Z., C.W., Z.B., Z.Y. (Zhisheng Yu) and F.L.; supervision, Z.S. and F.L.; project administration, Z.S., F.L. and G.Z.; funding acquisition, G.Z. All authors have read and agreed to the published version of the manuscript.

Funding: National Major Science and Technology Program (No. 2018ZX07110-002) for Water Pollution Control and Treatment. Henan Province Key Research and Development and Promotion Special (No. 182102311016).

Institutional Review Board Statement: Not applicable.

Informed Consent Statement: Not applicable.

Data Availability Statement: The data presented in this study are available on request from the corresponding author.

Acknowledgments: The authors gratefully acknowledge the funding support provided by National Major Science and Technology Program (No. 2018ZX07110-002) for Water Pollution Control and Treatment and Henan Province Key Research and Development and Promotion Special (No. 182102311016).

Conflicts of Interest: The authors declare no conflict of interest.

References

1. Keimowitz, A.R.; Zheng, Y.; Chillrud, S.N.; Mailloux, B.; Jung, H.B.; Stute, M.; Simpson, H.J. Arsenic Redistribution between Sediments and Water near a Highly Contaminated Source. *Environ. Sci. Technol.* **2010**, *39*, 8606–8613. [CrossRef] [PubMed]
2. Yu, H.S.; Lee, C.H.; Chen, G.S. Peripheral vascular diseases resulting from chronic arsenical poisoning. *J. Dermatol.* **2002**, *29*, 123–130. [CrossRef] [PubMed]
3. Antman, K.H. Introduction: The history of arsenic trioxide in cancer therapy. *Oncologist* **2001**, *6*. [CrossRef] [PubMed]
4. Cullen, W.R.; Reimer, K.J. Arsenic speciation in the environment. *Chem. Rev.* **1989**, *89*, 713–764. [CrossRef]
5. Dixit, S.; Hering, J.G. Comparison of arsenic(V) and arsenic(III) sorption onto iron oxide minerals: Implications for arsenic mobility. *Environ. Sci. Technol.* **2003**, *37*, 4182–4189. [CrossRef] [PubMed]
6. Manning, B.A.; Martens, D.A. Speciation of arsenic(III) and arsenic(V) in sediment extracts by high-performance liquid chromatography-hydride generation atomic absorption spectrophotometry. *Environ. Sci. Technol.* **1997**, *31*, 171–177. [CrossRef]
7. Bothe, J.V.; Brown, P.W. The stabilities of calcium arsenates at 23 ± 1 °C. *J. Hazard. Mater.* **1999**, *68*, 197–207. [CrossRef]
8. Chiu, V.Q.; Hering, J.G. Arsenic adsorption and oxidation at manganite surfaces. 1. Method for simultaneous determination of adsorbed and dissolved arsenic species. *Environ. Sci. Technol.* **2000**, *34*, 2029–2034. [CrossRef]
9. Usman, M.; Katsoyiannis, I.; Mitrakas, M.; Zouboulis, A.; Ernst, M. Performance Evaluation of Small Sized Powdered Ferric Hydroxide as Arsenic Adsorbent. *Water* **2020**, *12*, 1430. [CrossRef]
10. Gupta, V.K.; Sharma, S. Removal of cadmium and zinc from aqueous solutions using red mud. *Environ. Sci. Technol.* **2002**, *36*, 3612–3617. [CrossRef] [PubMed]
11. Srivastava, S.K.; Gupta, V.K.; Mohan, D. Removal of lead and chromium by activated slag- a blast furnace waste. *J. Environ. Eng.* **1997**, *123*, 461–468. [CrossRef]
12. Mohan, D.; Pittman, C.J.; Bricka, M.; Smith, F.; Yancey, B.; Mohammad, J.; Steele, P.; Alexandre-Franco, M.F.; Gómez-Serrano, V.; Gong, H. Sorption of arsenic, cadmium, and lead by chars produced from fast pyrolysis of wood and bark during bio-oil production. *J. Colloid Interf. Sci.* **2007**, *310*, 57–73. [CrossRef] [PubMed]
13. Tennant, M.F.; Mazyck, D.W. Steam-pyrolysis activation of wood char for superior odorant removal. *Carbon.* **2003**, *41*, 2195–2202. [CrossRef]
14. Boni, M.R.; Marzeddu, S.; Tatti, F.; Raboni, M.; Mancini, G.; Luciano, A.; Viotti, P. Experimental and Numerical Study of Biochar Fixed Bed Column for the Adsorption of Arsenic from Aqueous Solutions. *Water* **2021**, *13*, 915. [CrossRef]
15. Ioannidou, O.; Zabaniotou, A. Agricultural residues as precursors for activated carbon production–A review. *Renew. Sust. Energ. Rev.* **2007**, *11*, 1966–2005. [CrossRef]
16. Demirbas, A. Effects of temperature and particle size on bio-char yield from pyrolysis of agricultural residues. *J. Anal. Appl. Pyrol.* **2004**, *72*, 243–248. [CrossRef]
17. Fierro, V.; Torné-Fernández, V.; Celzard, A. Kraft lignin as a precursor for microporous activated carbons prepared by impregnation with ortho-phosphoric acid: Synthesis and textural characterization. *Micropor. Mesopor. Mater.* **2006**, *92*, 243–250. [CrossRef]

18. Pillai, K.; Raizada, A. Modeling Transport and Adsorption of Arsenic Ions in Iron-Oxide Laden Porous Media. Part I: Theoretical Developments. *Water* **2021**, *13*, 779. [CrossRef]
19. Bae, J.; Kim, S.; Kim, K.S.; Hwang, H.K.; Choi, H. Adsorptive Removal of Arsenic by Mesoporous Iron Oxide in Aquatic Systems. *Water* **2020**, *12*, 3147. [CrossRef]
20. Kanel, S.R.; Manning, B.; Charlet, L.; Choi, H. Removal of Arsenic(III) from Groundwater by Nanoscale Zero-Valent Iron. *Environ. Sci. Technol.* **2005**, *39*, 1291–1298. [CrossRef]
21. Zhu, H.; Jia, Y.; Wu, X.; Wang, H. Removal of arsenic from water by supported nano zero-valent iron on activated carbon. *J. Hazard. Mater.* **2009**, *172*, 1591–1596. [CrossRef]
22. Van de Velde, K.; Kiekens, P. Structure analysis and degree of substitution of chitin, chitosan and dibutyrylchitin by FT-IR spectroscopy and solid state 13C NMR. *Carbohyd. Polym.* **2004**, *58*, 409–416. [CrossRef]
23. Furuhashi, T.; Beran, A.; Blazso, M.; Czegeny, Z.; Schwarzinger, C.; Steiner, G. Pyrolysis GC/MS and IR spectroscopy in chitin analysis of molluscan shells. *Biosci. Biotechnol. Biochem.* **2009**, *73*, 93–103. [CrossRef] [PubMed]
24. Juang, R.S.; Tseng, R.L.; Wu, F.C.; Lee, S.H. Adsorption behavior of reactive dyes from aqueous solutions on chitosan. *J. Chem. Tech. Biotechnol.* **1997**, *70*, 391–399. [CrossRef]
25. Vinokurov, I.A.; Jouko, K. Kinetics of Multilayer Langmuirian Adsorption. *Langmuir* **2002**, *18*, 6789–6795. [CrossRef]
26. Choi, J.; Choi, N.; Lee, S.; Kim, D. Novel three-stage kinetic model for aqueous benzene adsorption on activated carbon. *J. Colloid Interf. Sci.* **2007**, *314*, 367–372. [CrossRef] [PubMed]
27. Zhao, C.; Ping, G.; Zhang, G. A hybrid process of powdered activated carbon countercurrent two-stage adsorption and microfiltration for petrochemical RO concentrate treatment. *Desalination* **2013**, *330*, 9–15. [CrossRef]
28. Annadurai, G.; Ling, L.Y.; Lee, J. Adsorption of reactive dye from an aqueous solution by chitosan: Isotherm, kinetic and thermodynamic analysis. *J. Hazard. Mater.* **2008**, *152*, 337–346. [CrossRef]
29. Gutig, C.; Grady, B.P.; Striolo, A. Experimental Studies on the Adsorption of Two Surfactants on Solid−Aqueous Interfaces: Adsorption Isotherms and Kinetics. *Langmuir* **2008**, *24*, 13814. [CrossRef]
30. Day, J.P.R.; Campbell, R.A.; Russell, O.P.; Bain, C.D. Adsorption Kinetics in Binary Surfactant Mixtures Studied with External Reflection FTIR Spectroscopy. *J. Phys. Chem. C* **2007**, *111*, 8757–8774. [CrossRef]
31. Kern, M.E.; David, F.W. Influence of Dispersion Forces and Ordering on the Compositions of Mixed Monolayers of Alkanoic Acids on Nanocrystalline TiO2 Films. *Langmuir* **2013**, *29*, 13797–13807. [CrossRef]
32. Moorkanikkara, S.N.; Blankschtein, D. New Theoretical Framework for Designing Nonionic Surfactant Mixtures that Exhibit a Desired Adsorption Kinetics Behavior. *Langmuir* **2010**, *26*, 18728–18733. [CrossRef]
33. Yang, Z.; Zhang, B.; Chen, X.; Bai, Z.; Zhang, H. Studies on pyrolysis of wheat straw residues from ethanol production by solid-state fermentation. *J. Anal. Appl. Pyrolysis* **2008**, *81*, 243–246. [CrossRef]
34. Yang, Z.; Zhuang, G.; Bai, Z.; Zhang, H.; Guo, Y.; Dong, Y. Preparation and formation mechanism of levoglucosan from starch using a tubular furnace pyrolysis reactor. *J. Anal. Appl. Pyrolysis* **2013**, *102*, 83–88. [CrossRef]
35. Jin, H.; Capareda, S.; Chang, Z.; Gao, J.; Xu, Y.; Zhang, J. Biochar pyrolytically produced from municipal solid wastes for aqueous As(V) removal: Adsorption property and its improvement with KOH activation. *Bioresour. Technol.* **2014**, *169*, 622–629. [CrossRef] [PubMed]
36. Begum, S.A.; Golam Hyder, A.H.M.; Vahdat, N. Adsorption isotherm and kinetic studies of As(V) removal from aqueous solution using cattle bone char. *J. Water Supply Res. Technol. AQUA* **2016**, *65*, 244–252. [CrossRef]
37. Niazi, N.K.; Bibi, I.; Shahid, M.; Ok, Y.S.; Burton, E.D.; Wang, H.; Shaheen, S.M.; Rinklebe, J.; Lüttge, A. Arsenic removal by perilla leaf biochar in aqueous solutions and groundwater: An integrated spectroscopic and microscopic examination. *Environ. Pollut.* **2018**, *232*, 31–41. [CrossRef] [PubMed]
38. Sattar, M.S.; Shakoor, M.B.; Ali, S.; Rizwan, M.; Niazi, N.K.; Jilani, A. Comparative efficiency of peanut shell and peanut shellbiochar for removal of arsenic from water. *Environ. Sci. Pollut. Res.* **2019**, *26*, 18624–18635. [CrossRef]
39. Nishimura, T.; Robins, R.G. A Re-evaluation of the Solubility and Stability Regions of Calcium Arsenites and Calcium Arsenates in Aqueous Solution at 25°C, Mineral Processing and Extractive Metallurgy Review. *Min. Pro. Ext. Met. Rev.* **1998**, *18*, 283–308. [CrossRef]
40. Margulis, H.; Gane, J. Action of Lime on Arsenious Acid. *Annal. Agron.* **1948**, *18*, 28–32.
41. Masson, J.; Guérin, H. On the Alkali Earth Arsenites: Study of the Systems (Ba, Sr, Ca)O-As2O3-H2O. *Bull. Soc. Chim. France* **1958**, *1958*, 400–403.
42. Sethuraman, V.V.; Raymahashay, B.C. Color removal by clays. Kinetic study of adsorption of cationic and anionic dyes. *Environ. Sci. Technol.* **1975**, *9*, 1139–1140.
43. Alexander, F.; Poots, V.J.P.; McKay, G. Adsorption kinetics and diffusion mass transfer processes during color removal from effluent using silica. *Ind. Eng. Chem. Process. Des. Dev.* **1978**, *17*, 406–410. [CrossRef]